Annals of Biomedical Engineering, Vol. 19, pp. 679–697, 1991
Printed in the USA.

0090-6964/91 $3.00 + .00

Sensitivity of CO_2 Washout to Changes in Acinar Structure in a Single-Path Model of Lung Airways

Jeffrey D. Schwardt,* Sherif R. Gobran,*‡ Gordon R. Neufeld,†‡
Stanley J. Aukburg,† and Peter W. Scherer*†

*Department of Bioengineering, School of Engineering and Applied Science, University of Pennsylvania, Philadelphia, PA
†Department of Anesthesia, University of Pennsylvania, School of Medicine, Philadelphia, PA
‡Philadelphia Veterans Affairs Medical Center, Philadelphia, PA

(Received 7/5/90; Revised 3/19/91)

A numerical solution of the convection-diffusion equation with an alveolar source term in a single-path model (SPM) of the lung airways simulates steady state CO_2 washout. The SPM is used to examine the effects of independent changes in physiologic and acinar structure parameters on the slope and height of Phase III of the single-breath CO_2 washout curve. The parameters investigated include tidal volume, breathing frequency, total cardiac output, pulmonary arterial CO_2 tension, functional residual capacity, pulmonary bloodflow distribution, alveolar volume, total acinar airway cross sectional area, and gas-phase molecular diffusivity. Reduced tidal volume causes significant steepening of Phase III, which agrees well with experimental data. Simulations with a fixed frequency and tidal volume show that changes in bloodflow distribution, model airway cross section, and gas diffusivity strongly affect the slope of Phase III while changes in cardiac output and in pulmonary arterial CO_2 tension strongly affect the height of Phase III. The paper also discusses differing explanations for the slope of Phase III, including sequential emptying, stratified inhomogeneity, and the issue of asymmetry, in the context of the SPM.

Keywords—*Convection, Diffusion, Pulmonary gas exchange, Numerical model, Phase III slope.*

INTRODUCTION

The CO_2 expirogram is a plot of gas concentration versus expired volume and is customarily divided into three phases as shown in Fig. 1. Phase I is the washout of the uppermost conducting airways and is almost completely free of CO_2. Phase II is the rapidly rising portion of the curve and Phase III, also known as the alveolar plateau, represents gas contained in the acini or peripheral alveolated airways. Phase III contains most of the exhaled CO_2 and is usually characterized by a relatively linear increase in concentration versus exhaled volume (8). The cause of the Phase III slope

Acknowledgment—These studies were supported by the National Heart, Lung, and Blood Institute Grant HL-33891 and the Veterans Administration Merit Review Grant (103).

Address correspondence to Dr. Peter W. Scherer, Department of Bioengineering, University of Pennsylvania, 220 South 33rd Street, Philadelphia, PA 19104.

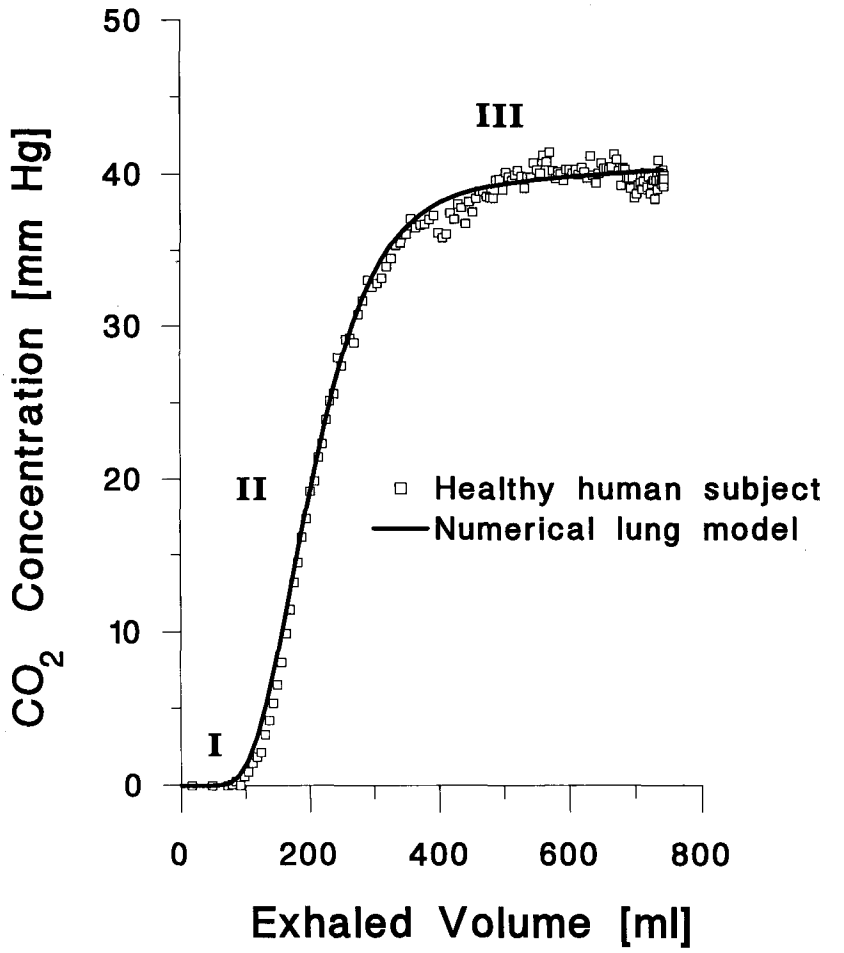

FIGURE 1. Experimentally measured CO_2 washout from a healthy human subject (with FRC = 3307 ml, V_T = 742 ml, and f = 10.3 bpm) is compared to a computed washout curve obtained from the SPM. Note the distinct phases I, II, and III marked on the tracings.

of gas washout curves recorded at the mouth has been a subject of debate for many years.

Three explanations have been offered: (a) sequential or out-of-phase emptying of different parallel lung regions, each containing different concentrations of the measured gas (28); (b) continuing evolution of gas from the blood into a contracting alveolar volume (5,7); and (c) the presence of longitudinal gas concentration gradients in the airways (stratified inhomogeneity) due to a combination of factors such as gas convection, molecular diffusion, airway geometry, and gas evolution from the blood (6,18,22). The third explanation, based on stratified inhomogeneity, is presented here as the solution of the airway convection-diffusion equation in a symmetric single-path trumpet bell model (SPM). The SPM has been proposed to explain many features of the normal expirogram and steady state gas elimination (18,22). Refer to the Discussion section for a detailed comparison of the explanations of Phase III slope and com-

ments on the adequacy of the SPM to represent gas washout in the real asymmetric airway system.

Anatomic dimensions for the standard healthy lung model are taken from Weibel's symmetric Model A (25) which specifies airway length, diameter, and number of alveoli per generation for 23 generations of dichotomous branching airways. The conducting airways are represented by generations $z = 0$–16 and the alveolated airways by generations $z = 17$–23. In the computer model, airway volume $V(z)$ is held constant and inhalation and exhalation of the tidal volume V_T is accomplished by expansion and contraction of the surrounding alveolar volume $V_A(z,t)$. Figure 2 shows the distinction between airway and alveolar volumes in the lung model. The airway cross section $A(z)$ in the SPM is the summed cross section of all branches in generation z. Airway anatomic models similar to Weibel's have been developed more recently (9,10), however, the original Weibel model was chosen for this study because it represents the oldest and best known symmetric morphological model of the lung airways and provides a good starting point for parameter sensitivity studies.

METHODS

Carbon dioxide transport in the airways is simulated by performing a mass balance across a slice of the trumpet bell model (18) to yield the airway convection-diffusion equation

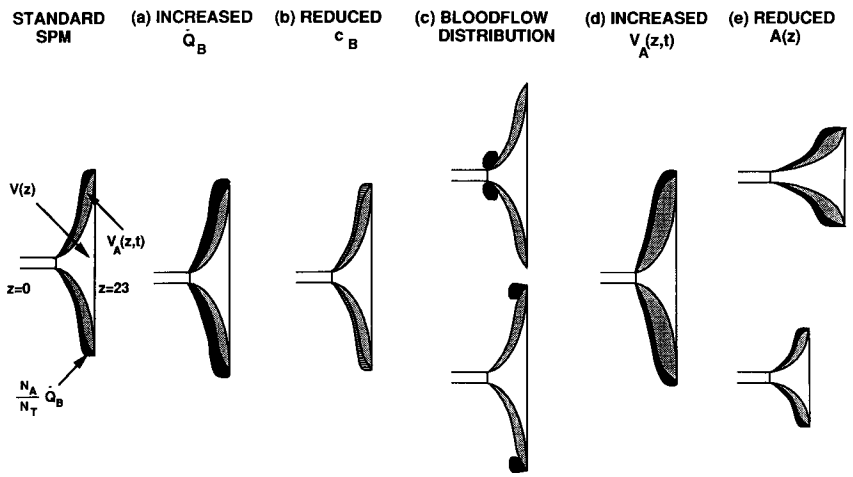

FIGURE 2. Standard SPM is illustrated along with some schematic examples of variations of model parameters. During simulated breathing, the airway volume $V(z)$ is held constant and the surrounding alveolar volume $V_A(z,t)$ expands in proportion to the number of alveoli in each generation to allow for inhalation of tidal volume. Evolution of CO_2 from the blood into the alveolated airways is proportional to the total cardiac output $\dot{Q}_B$ and the number fraction of alveoli in each generation N_A/N_T (a) shows increased cardiac output; (b) shows reduced pulmonary arterial blood CO_2 tension; (c) shows two extreme bloodflow redistributions; (d) shows increased alveolar volume; and (e) shows reduced airway cross section both with and without airway lengthening.

$$\left(1 + \frac{V_A}{V}\right)\frac{\partial c}{\partial t} + \left(\frac{\dot{Q}}{V}\right)\frac{\partial c}{\partial z} = \frac{1}{V}\frac{\partial}{\partial z}\left[\frac{D_{\text{mol}}A}{l}\frac{\partial c}{\partial z}\right] + \frac{S}{V} \tag{1}$$

and appropriate boundary conditions (18). (See Nomenclature for symbol definitions.)

The last term on the right in Eq. 1 is a source term that represents CO_2 evolution from the blood into the lung airspace according to the local bloodflow distribution. Pulmonary bloodflow distribution in the SPM is based on the number of alveoli in each generation of the Weibel lung (25) and the evolution of CO_2 from the blood is described by (18)

$$S(z) = \frac{N_A(z)}{N_T}\dot{Q}_B\lambda(\sqrt{c_B} - \sqrt{c}) \ . \tag{2}$$

If Eq. 1 is integrated from a given generation z to the end of the model at $z = 23$ and the resulting equation is rearranged and solved for $\partial c/\partial V = (1/Al)(\partial c/\partial z)$, one obtains

$$\left.\frac{\partial c}{\partial V}\right|_z = \frac{1}{D_{\text{mol}}A^2|_z}\left[\dot{Q}c|_z - \int_{\Delta z}\left[[V + V_A]\frac{\partial c}{\partial t}\right]dz + \int_{\Delta z} S[z,t]dz\right] \ . \tag{3}$$

Equation 3 shows that at any instant the slope, $\partial c/\partial V$, of the concentration profile at a given point z in the airways is especially sensitive to the total airway cross section $A(z)$ and the blood source emission rate.

Dimensions of the standard model lung used in this study were derived from the morphometric data of Weibel's model A (25) which were obtained from measurements on a human lung at 3/4 inflation, with a total airspace volume of 4800 ml. This volume is much larger than the normal functional residual capacity (FRC) in man. A typical adult male human lung has an FRC of only 2500 ml (26). Airway dimensions for the numerical model were therefore reduced by isometrically scaling the airways of Weibel generations 5–23 by using the following formulas:

$$A_{\text{model}}(z) = A_{\text{Weibel}}(z)(SF)^{2/3} \ , \qquad z > 4 \tag{4a}$$

$$l_{\text{model}}(z) = l_{\text{Weibel}}(z)(SF)^{1/3} \ , \qquad z > 4 \tag{4b}$$

where SF is a scaling factor defined as

$$SF = \frac{\text{FRC}_{\text{model}} - V_c + \frac{V_T}{2}}{\text{FRC}_{\text{Weibel}} - V_c} \tag{4c}$$

with $\text{FRC}_{\text{model}} = 2500$ ml for a healthy model lung, $\text{FRC}_{\text{Weibel}} = 4800$ ml, and V_c as the volume of the conducting airways of generation 0–4. Model generations 0–4 were unaltered because they represent the more rigid airways of the mouth, nose, and main bronchi. The airways of generations 5–23 were sized according to an assigned $\text{FRC}_{\text{model}}$ plus $V_T/2$ in order to approximate the average distention that occurs during a breath of volume V_T. After scaling airway dimensions, alveolar volumes were assigned according to the number of alveoli in each Weibel generation.

Using the SPM, we examined changes in numerically-calculated CO_2 washout due to variations in model parameters. These simulation experiments were compared to the calculated gas exchange in a standard or normal lung with a standard breathing pattern. Adjustable parameters and physiologic variables in the SPM include V_T, breathing frequency f, total cardiac output $\dot{Q}_B$, pulmonary arterial CO_2 tension c_B, FRC, pulmonary bloodflow distribution $(N_A/N_T)\dot{Q}_B$, total alveolar volume at the beginning inspiration of $V_{A,T}$, airway cross-sectional area $A(z)$, and gas-phase molecular diffusivity D_{mol}.

Standard values of physiologic and structural parameters were chosen consistent with normal breathing in a healthy adult male (3,26). Normal breathing is simulated with a symmetric sinusoidal air-flow pattern at the mouth with $V_T = 750$ ml, $f = 12$ breaths per minute (bpm), $\dot{Q}_B = 6.6$ l/min, and $c_B = 48$ mm Hg in a SPM with FRC = 2500 ml. Standard bloodflow distribution is based on the values of N_A and N_T from Weibel's model A (25). The standard value for $V_{A,T}$ is the difference between the FRC and the total airway volume of the scaled Weibel geometry, which results in $V_{A,T} = 1440$ ml. $A(z)$ for the standard SPM is also determined according to the scaled Weibel geometry and $D_{mol} = 0.17$ cm^2/s, the value for CO_2 in alveolar air (29).

For each parameter sensitivity test, one parameter was varied through a range of values while all other parameters were held constant according to the standard model lung described above. Some examples of acinar structure changes are shown schematically in Fig. 2.

Tidal volume was varied through the range $350 < V_T < 1250$ ml.

Breathing frequency was varied through the range $4 < f < 22$.

Total cardiac output was varied through the range $1.8 < \dot{Q}_B < 13.2$ l/min. The parameter ranges for V_T, f, and $\dot{Q}_B$ were chosen to be consistent with the breathing patterns and cardiac output of a healthy adult male at rest and during moderate exercise (3).

Pulmonary arterial CO_2 tension was varied through the range $36 < c_B < 60$ mm Hg. This range of c_B represents the conditions of hypocapnia and hypercapnia measured in healthy subjects during exercise and in patients with severe emphysema (3,13).

FRC was varied through the range 1500 < FRC < 3500 ml. Changes in FRC cause corresponding changes in prescribed airway dimensions according to Eq. 4. This range for FRC was chosen to be consistent with the lung volume increases associated with obstructive lung disease (4).

Bloodflow distribution was changed from the standard Weibel distribution by varying the fraction N_A/N_T in Eq. 2 which then changed the distributed source $S(z)$. The alveolar volume in each generation was not changed during this parameter sensitivity test—only the bloodflow in each generation was varied. For instance, perfusion can be diverted to more proximal generations by cutting off bloodflow to generation 23 and redistributing cardiac output among the remaining generations 17–22. A range of perfusion distributions was generated in this way, with the extreme distributions of all bloodflow to generation 17 or all bloodflow to generation 23 (Fig. 2).

Alveolar volume was varied through the range $400 < V_{A,T} < 2800$ ml. Like the range of FRC values, this range for $V_{A,T}$ was chosen according to increases in lung volume associated with obstructive lung disease (4).

Total airway cross section $A(z)$ was varied by multiplying the areas in generations 17–23 by a constant area reduction factor R. $R = 1.0$ in the healthy standard SPM.

R was varied through the range $0.5 < R < 2.0$, which includes both airway constriction and dilation. This range was chosen based on an analysis of the differences between healthy and emphysematous lung tissues. Patients with emphysema have a reduced number of abnormally large respiratory airspaces (as shown in the micrographs of Fig. 3) and an increased FRC (1). An area reduction factor can be derived for the disease state by idealizing human lung morphology as a collection of spherically shaped airspaces grouped sequentially in the acinar generations of a SPM. The number of such spheres in each generation of the healthy standard lung model is

$$N_H(z) = \frac{[V_{\text{airway}}(z) + V_{\text{alveolar}}(z)]}{\frac{\pi}{6} d_H^3}$$

and the number of spherical airspaces in the diseased lung is

$$N_D(z) = \frac{\alpha[V_{\text{airway}}(z) + V_{\text{alveolar}}(z)]}{\frac{\pi}{6} d_D^3}$$

where $\alpha = \text{FRC}_D/\text{FRC}_H$, the ratio of diseased to healthy functional residual capacities. By approximating longitudinal diffusing area in each airspace as the maximum cross section of the sphere, the total cross sectional area in each generation of the healthy and diseased lungs can be expressed as

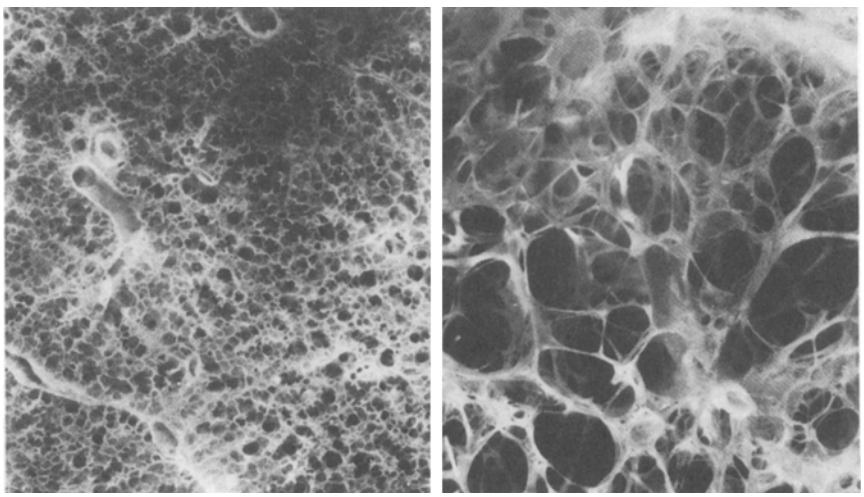

FIGURE 3. Micrographs of a normal lung (left) and a lung known to have panlobular emphysema (right). Both images are magnified 10×. Note the dramatic increase in airspace sizes between health and disease. [From Heard, B.E. Pathology of Chronic Bronchitis and Emphysema, London: Churchill; 1969.]

$$A_H(z) = N_H(z)\,\frac{\pi d_H^2}{4} \qquad \text{and} \qquad A_D(z) = N_D(z)\,\frac{\pi d_D^2}{4}\ .$$

By defining the ratio of diseased to healthy airspace diameters as $\beta = d_D/d_H$, the total airway cross section of the diseased and healthy lung structures can be compared in terms of the two ratios α and β. The resulting area reduction factor is

$$R = \frac{\alpha}{\beta} = \frac{A_D(z)}{A_H(z)}\ .$$

Airspace sizes measured from micrographs of excised lung sections, such as those shown in Fig. 3, have typical airspace diameters ranging from $d_H = 0.2$ mm in a healthy lung to $d_D = 1.33$ mm in a lung with severe panlobular emphysema (1,27). Appropriate values for α and β are in the ranges $1 < \alpha < 1.7$ and $1 < \beta < 5$, which result in area-reduction factors in the range $0.2 < R < 1.7$. This implies that the total mouthward cross-sectional diffusing area for CO_2 in a severely diseased lung may be as small as one fifth of that in a healthy lung. In order to preserve the total airway volume $V(z)$ in each generation, airway lengths $l(z)$ were increased in generations 17–23 as $A(z)$ was decreased. This maintains tidal volume penetration to the same generational depth in an area-reduced lung as in the standard lung. A group of simulations was also done in which airways were not lengthened. Area reduction without airway lengthening causes the tidal volume to penetrate to deeper generational depths than airway reduction with lengthening.

Diffusivity was varied through the range $0.05 < D_{\text{mol}} < 0.8$ cm^2/s. This covers a range of tracer gases familiar to the pulmonary physiologist including SF_6 ($D_{SF_6\text{–air}} = 0.103$ cm^2/s), CO_2($D_{CO_2\text{–air}} = 0.17$ cm^2/s), and He ($D_{\text{He–air}} = 0.74$ cm^2/s) (29).

All airways have an initial CO_2 concentration in equilibrium with the pulmonary arterial blood, that is $c(z, t = 0) = c_B$. After steady state had been attained (usually ~3 breaths) in each numerical breathing simulation, the Phase III slope $dc/dV|_{\text{III}}$ and the minute CO_2 excretion $\dot{V}_{CO_2}$ were calculated. Phase III is defined as a fixed range of the washout tracing. The midpoint of Phase III is positioned at the volume containing 60% of exhaled CO_2. Phase III slope is then computed by linear regression on points ±35% of the calculated alveolar volume, which was calculated using the Bohr equation (2). $\dot{V}_{CO_2}$ is the product of the area under the washout curve and the breathing frequency.

RESULTS

The standard model lung produces a Phase III slope of 0.76 %/l, a $\dot{V}_{CO_2}$ of 378 ml/min, and an end tidal CO_2 concentration of 42.0 mm Hg, in good agreement with mean values measured on healthy human subjects breathing normally at rest in our pulmonary laboratory (14). Results of the parameter sensitivity studies will be presented in two groups—the sensitivity to breathing pattern (V_T and f), followed by the sensitivity to other structural and physiologic parameters.

Reduced V_T causes significant Phase III steepening to values as high as 6.7 %/l when $V_T = 350$ ml (Fig. 4). Figure 4 also shows the agreement between the SPM and 671 Phase III slopes measured from 6 healthy volunteers breathing normally at rest with tidal volumes between 5 and 23 ml/kg body weight (14). The measured slopes

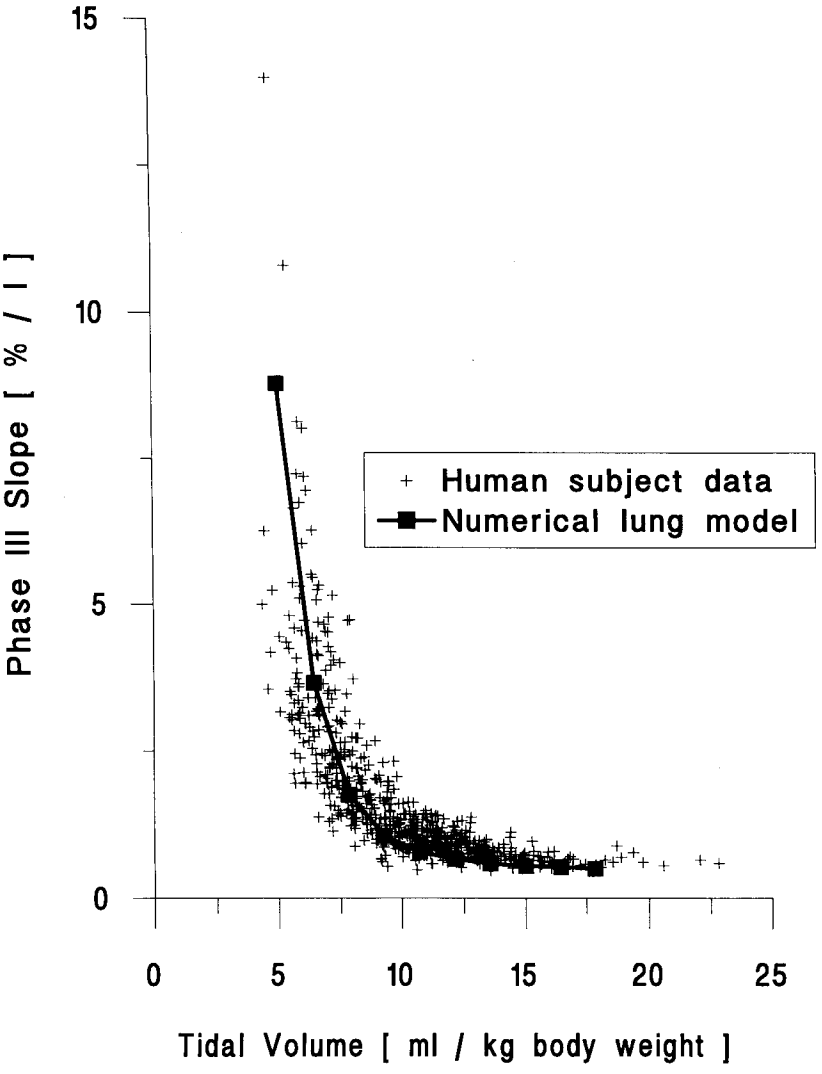

FIGURE 4. Comparison of the SPM and experimentally measured Phase III slopes versus tidal volume from 6 healthy volunteers. The numerical data shown is that of the standard model lung with FRC = 2500 ml and an assumed body weight of 70 kg.

are plotted against the measured tidal volume per kg body weight and compared to the SPM data (assuming a body weight of 70 kg for the SPM data). The trend of rapidly decreasing slope with V_T is observed, just as the SPM predicts. As V_T goes from 350 to 1250 ml, $\dot{V}_{CO_2}$ increases linearly from 148 to 627 ml/min. As f goes from 4 to 22 bpm, Phase III slope increases only slightly from 0.6 to 1.1 %/l and $\dot{V}_{CO_2}$ rises linearly from 131 to 670 ml/min.

By far the largest increase in Phase III slope due to a structure change is caused by area reduction with airway lengthening, which results in slopes as high as 2.4 %/l with an area reduction factor of $R = 0.5$. Decreasing D_{mol} below the value for CO_2

in alveolar air also strongly increases Phase III slope to 2.0 %/l, as expected from Eq. 3 and shown in Fig. 5. In Fig. 6, the washout curve from the area-reduced lung with airway lengthening has the most obvious Phase III steepening compared to the standard washout curve. More modest Phase III steepening, with slopes only as high as 1.1 %/l, occurs as a result of area reduction without airway lengthening, increased

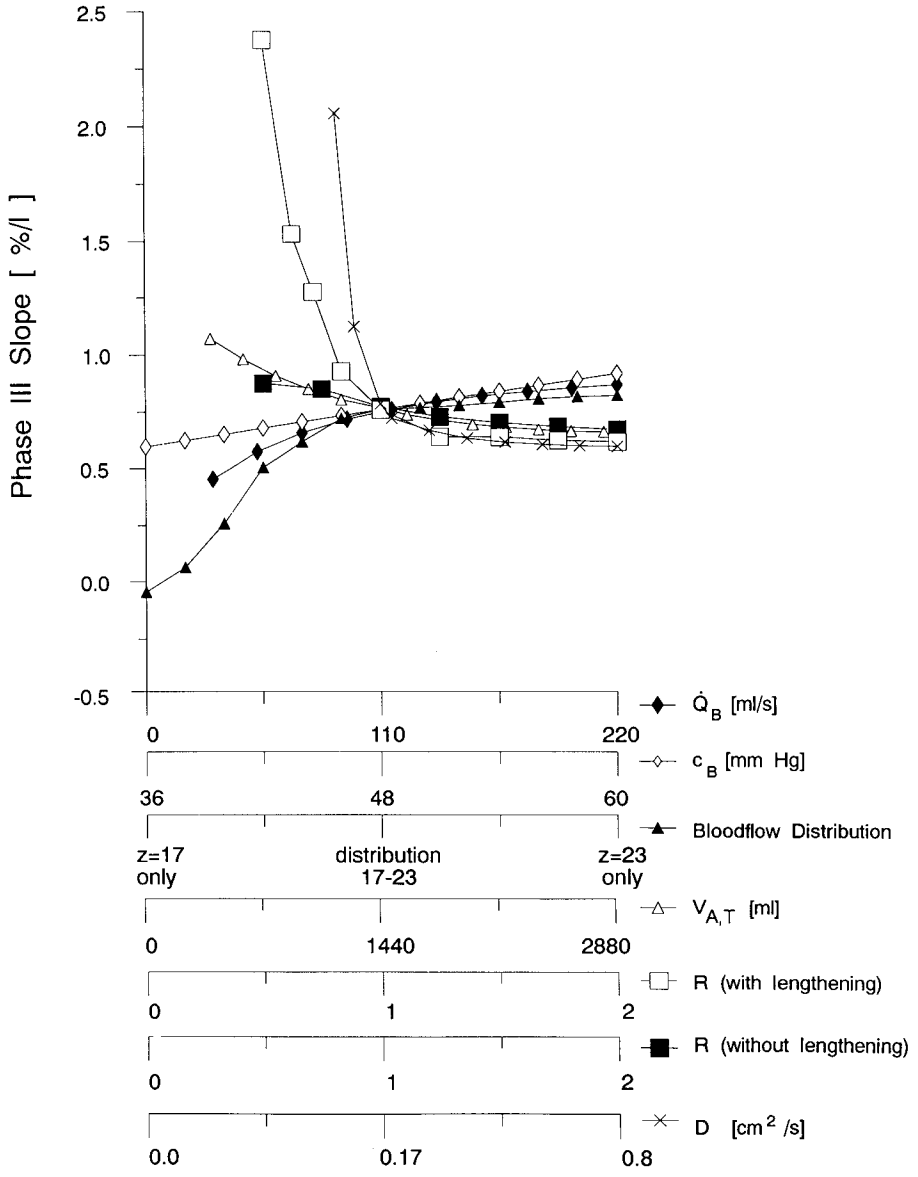

FIGURE 5. Sensitivity of Phase III slope to changes in physiologic and acinar structure parameters. All curves intersect at their normal values.

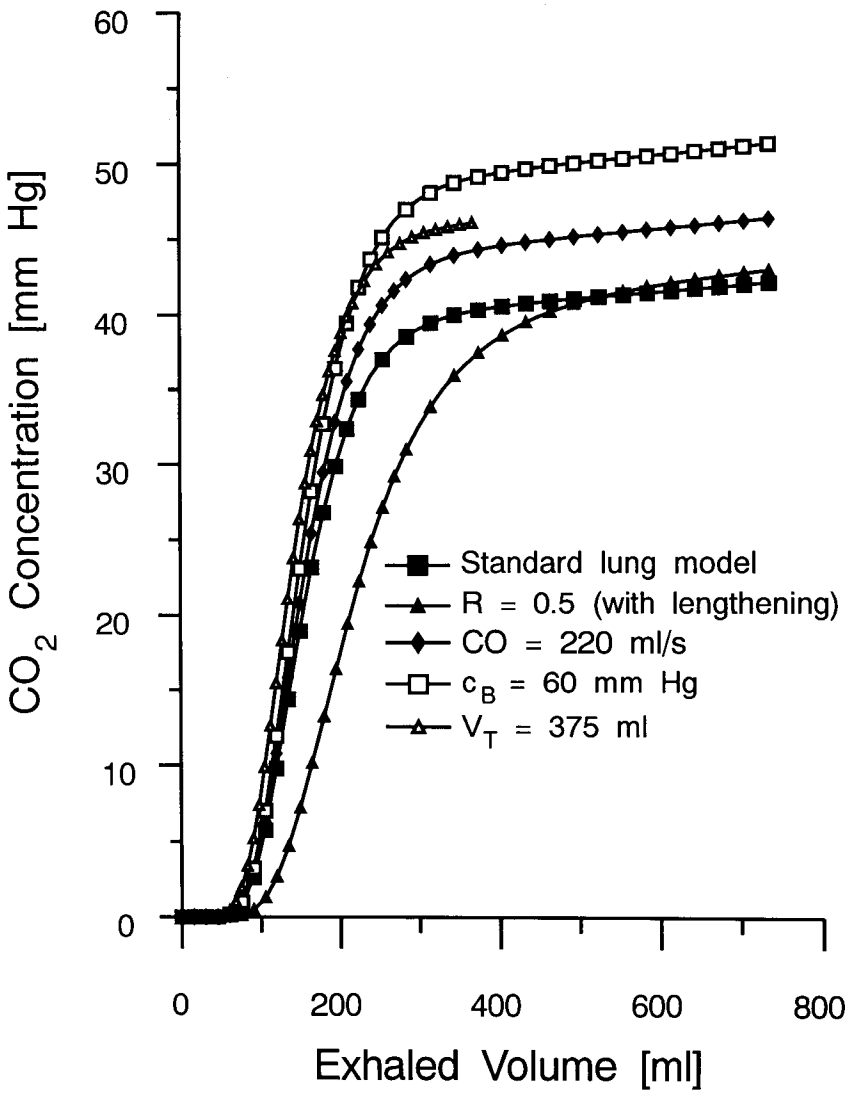

FIGURE 6. Specific examples from Fig. 5 of computed CO_2 washout curves that exhibit Phase III steepening.

cardiac output, increased pulmonary arterial blood CO_2 tension, increased FRC, and reduced alveolar volume.

The most significant Phase III flattening due to a SPM structure change occurs when all bloodflow is diverted to the most proximal alveolated generation 17, with a slightly negative calculated slope of −0.04 %/l. This flattened CO_2 washout is the uppermost curve in Fig. 7 and corresponds to the leftmost point on the associated sensitivity curve in Fig. 5. Less significant Phase III flattening, with slopes only as low as 0.5 %/l, occurs for cases of area dilation with and without airway shortening, reduced cardiac output, reduced blood CO_2 tension, reduced FRC, and increased al-

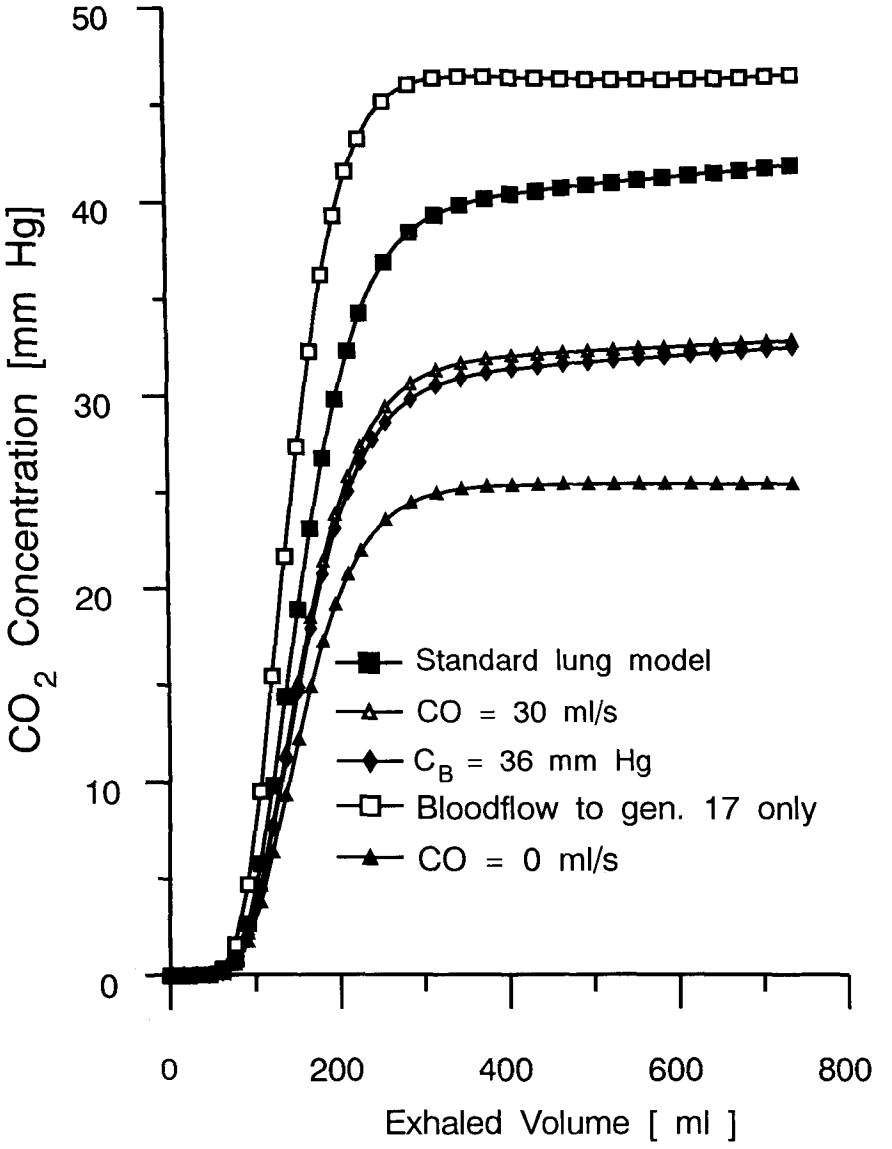

FIGURE 7. Specific examples from Fig. 5 of computed CO_2 washout curves that exhibit Phase III flattening.

veolar volume. Figure 7 also includes a washout curve from a lung with zero cardiac output, in which the source term $S(z,t)$ is eliminated, resulting in a nearly horizontal Phase III slope of 0.17 %/l. In this case, the only CO_2 in the lung is that specified by the initial conditions of the SPM simulation, and each breath depletes the residual CO_2.

Substantial increases in $\dot{V}_{CO_2}$ occurred when cardiac output was increased, blood CO_2 tension was increased, or all bloodflow was diverted to generation 17 as shown

in Fig. 8. As cardiac output is increased from 30 to 220 ml/s in the model, $\dot{V}_{CO_2}$ increases from 299 to 416 ml/min. As blood CO_2 tension is raised from 36 to 60 mm Hg, minute CO_2 excretion increases linearly from 293 to 461 ml/min. The simulation with all bloodflow to generation 17 resulted in elevation of the alveolar plateau to an end-tidal CO_2 tension of 46.6 mm Hg and $\dot{V}_{CO_2}$ of 443 ml/min, but $\dot{V}_{CO_2}$ decreases only to 372 ml/min as bloodflow is diverted to the most distal generation 23.

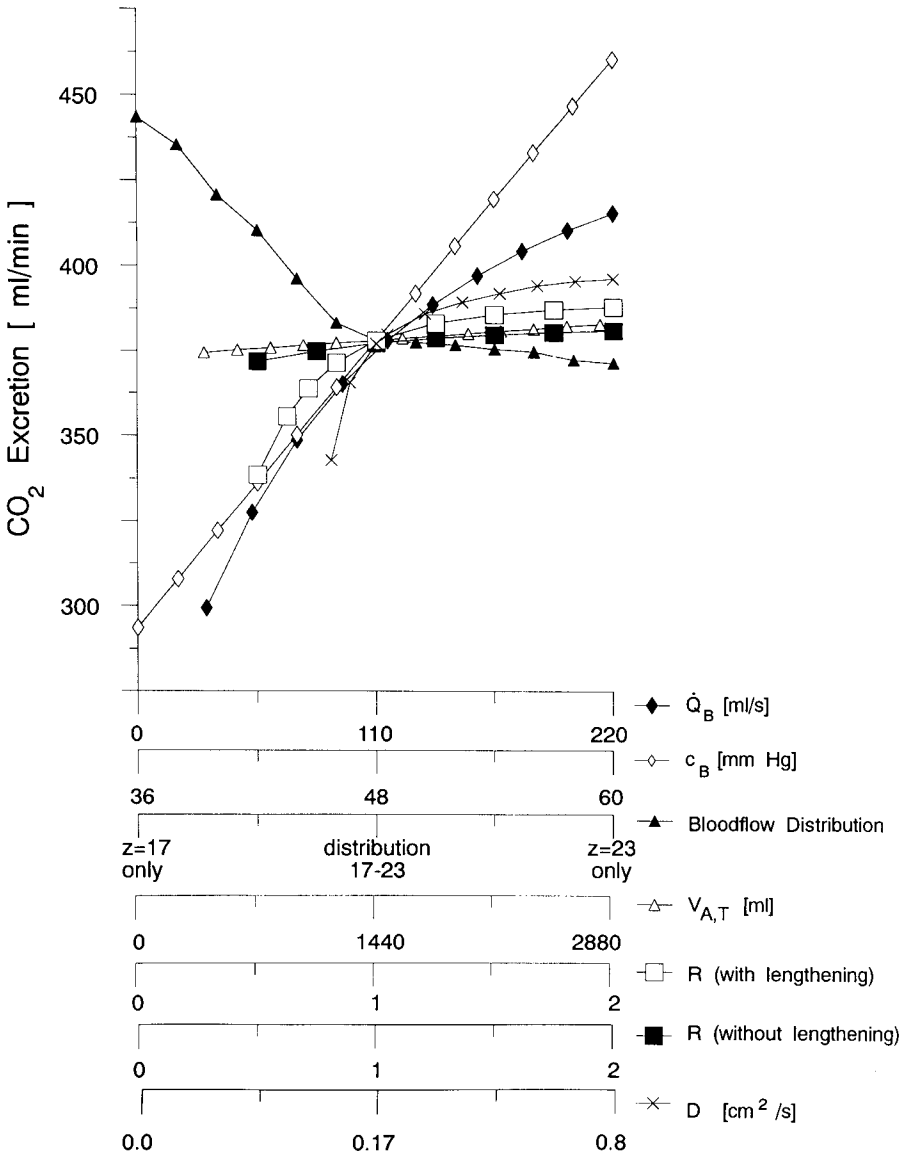

FIGURE 8. Sensitivity of $\dot{V}_{CO_2}$ to changes in physiologic and acinar structure parameters. Parameter ranges are identical to those plotted in Fig. 5.

Significant reduction of $\dot{V}_{CO_2}$ occurred due to airway reduction with lengthening, reduced cardiac output, and reduced blood CO_2 concentration. Changing the airway reduction factor with lengthening from $R = 2.0$ to $R = 0.5$ causes CO_2 excretion to drop by 31% from 388 to 267 ml/min. Area reduction without lengthening results in deviations of only ±10% from standard minute CO_2 excretion. $\dot{V}_{CO_2}$ is nearly unaffected by changes in alveolar volume, airway reduction without lengthening, FRC, or redistributing bloodflow toward the more distal alveolated generations.

Figure 1 shows a simulation in which the SPM is matched to a typical experimental washout curve from a healthy volunteer (14). The match was made by first setting experimentally measurable SPM parameters. For this subject, these parameter values are FRC = 3307 ml, $V_T = 742$ ml, and $f = 10.3$ bpm. While all other model parameters were fixed at their standard values, c_B was incremented during successive numerical simulations until the calculated end-tidal CO_2 concentration matched experiment. Next, R was incremented (with airway lengthening) until the calculated Phase III slope matched experiment. The resulting matching parameters are $c_B =$ 46.0 mm Hg and $R = 1.0$.

DISCUSSION

Due to the very small convective velocities in the lung periphery, gas transport by diffusion is the dominant mechanism in the acinar airways. Steepened Phase III slopes represent increased diffusional resistance in the peripheral lung airways. These steepened slopes occur when breathing involves a smaller than normal maximum interfacial area between the tidal volume and the FRC during a respiratory interval. Small tidal volumes produce steeper slopes because the inhaled air penetrates to shallower than normal depths in the lung and therefore encounters smaller than normal maximum interfacial areas and longer gas-phase diffusion paths. Area reduction with airway lengthening also results in a smaller maximum interfacial area and longer diffusion paths, thus increasing diffusional resistance to CO_2 transport and steepening Phase III slopes. Area reduction without airway lengthening results in nearly normal Phase III slopes because the V_T-FRC interface then penetrates deeper into the lung and encounters larger airway cross sectional areas and shorter diffusion path lengths. The weak dependence of Phase III slope on breathing frequency indicates that shorter transport times have only a minor effect on Phase III steepening. The slope changes by less than 50% of the standard value when frequency goes from 4 to 22 bpm and tidal volume is fixed. This represents a range of breathing periods from 15 seconds to less than 2 seconds in the SPM.

Flattened Phase III slopes result primarily from bloodflow redistribution toward more proximal alveolated generations. In the most extreme case, in which all bloodflow is diverted to generation 17, the tidal volume penetrates well beyond generation 17 into more distal acinar airways. A reverse diffusion gradient along the acinar airways occurs because tidal air is inhaled peripheral to the concentrated CO_2 source in generation 17. This gradient expresses itself on the washout curve as a downward sloping alveolar plateau and as an increased end-tidal CO_2 tension. This variant of bloodflow distribution demonstrates the trend toward higher CO_2 output and relatively flat or negative Phase III slope as bloodflow is directed away from the most peripheral generations of the lung model and toward the proximal alveolated airways.

Diverting all bloodflow to the most distal generation 23 results in CO_2 washout

nearly identical to the standard conditions. This is expected since according to Weibel's morphometric data, 76% of all alveoli reside in generations 22 and 23, with 48% in generation 23 (25). The largest portion of pulmonary circulation is directed to the most distal generations even in the standard case. The standard tidal volume of 750 ml penetrates only to airways in generation 22. The slightly increased average diffusion distance between blood source and the tidal volume-FRC interface does little to change the gas transport behavior when all bloodflow is diverted to generation 23. CO_2 washout with $\dot{Q}_B = 0.0$ causes Phase III to flatten appreciably (Fig. 7). This is due to the very small concentration gradient in the lung periphery in the absence of CO_2 evolution from the blood and is similar to the flat Phase III slopes generated by other single-path lung models that do not include the distributed CO_2 source term (15,22). The lower value of end-tidal CO_2 concentration on this curve (= 25.5 mm Hg) results because, without gas evolution from the blood, CO_2 is depleted from the initial concentration in the lung airways.

The height of the simulated alveolar plateau is affected primarily by $\dot{Q}_B$ or c_B when a normal breathing pattern and bloodflow distribution are assumed. Variations in $\dot{Q}_B$ and c_B in the model cause changes in Phase III amplitude but do not significantly alter Phase III slope, while mouthward bloodflow redistribution in the model causes both an increased amplitude and significantly flatter or negative slopes. The parameter-matching shown in Fig. 1 and the overlay of numerical and experimental data in Fig. 4, suggest that the SPM may be useful for understanding how acinar structural changes affect the CO_2 washout curve.

The SPM does not include parallel sequential emptying, which has been proposed as the basic mechanism for the sloping Phase III in spite of the contradictions predicted by the classical physiological theory when N_2 and CO_2 washout are considered in normal subjects. Sequential emptying is most often used to explain the upward sloping alveolar plateau of the single-breath nitrogen washout curve which is observed on expiration after the inhalation of a breath of pure oxygen (28). It is argued that during a normal inspiration from functional residual capacity in a healthy upright subject, the inspired O_2 goes preferentially to acini in the lung base, creating a vertical N_2 gradient at end inspiration with a greater N_2 concentration in the lung apex than in the base. During expiration, acini in the lung base are assumed to empty first followed by those in the apex, thus producing the rising N_2 alveolar plateau measured at the mouth.

This sequential emptying idea cannot simultaneously explain the shape of both the CO_2 and N_2 washout curves. A contradiction arises based on the well-established finding (26) that in a healthy upright individual during normal breathing, the CO_2 concentration is lower in acini located in the apex of the lung, where $P_{A_{CO_2}} \cong 30$ mm Hg, than in acini located in the base, where $P_{A_{CO_2}} \cong 42$ mm Hg. This vertical concentration gradient occurs because of the inequality between air ventilation and blood perfusion that exists normally in the upright lung. Sequential emptying of the airways in the same sequence as in the N_2 washout case, with the apex emptying last, would result in a CO_2 washout curve recorded at the mouth with a downward-sloping alveolar plateau rather than the upward-sloping alveolar plateau that is almost always observed experimentally.

Another explanation of the Phase III slope postulates that, during expiration, steady evolution of gas at the alveolar membrane into a well-mixed contracting alveolar volume results in a steady rise in gas concentration seen at the mouth (5,7).

However, this idea does not explain published observations of CO_2 washout from patients with severe emphysema. These expirograms generally have much steeper Phase III slopes than normals (8,23). Since the residual volume and FRC are greatly increased in patients with severe emphysema while the evolution and absorption rates of CO_2 and O_2 are about the same as normals, these gases are being excreted into or absorbed from larger peripheral volume reservoirs in the diseased state. During expiration, the gas concentrations in these larger volume reservoirs should therefore change more slowly with time or cumulative expired volume, not more rapidly as observed.

The SPM, which leads to the idea of stratified inhomogeneity or longitudinal airway concentration gradients, is based on the assumptions that (a) the spatial average concentration in the airways of the real lung is very close to the measured volume flow-weighted average concentration at the mouth; and (b) the degree of asymmetry in the real lung is small compared to the total airway path length or volume.

The first assumption of the SPM is supported by computing the difference between the experimentally measured volume flow-weighted average concentration and the spatial average gas concentration in an equivalent single path model. The SPM assumes spatial averaging of all airway paths between the mouth and the lung acini. The flow-weighted average concentration is what is actually measured at the mouth during expiration as a large number of lung regions empty simultaneously. Assuming that complete convective mixing predominates as gas streams from different regions come together on expiration at bronchial bifurcations (20,24), the flow weighted average seen at the mouth is given by (21)

$$\bar{c}_{fw} = \sum_{i=1}^{N} \frac{q_i c_i^0}{Q_{\text{tot}}} \tag{5}$$

where q_i and c_i^0 are the gas volume flow rate and concentration at the beginning of expiration in the ith alveolar duct (for washout of the alveolar plateau), $Q_{\text{tot}} = \sum q_i$ is the total expiratory volume flow rate out of the lung and N is the total number of alveolar ducts (ADs) emptying at a given instant or given expired volume. N is very large for washout of the alveolar plateau (e.g., $N \cong 10^7$ in Weibel's morphometric model). For this reason it is convenient to replace the summation in Eq. 5 with an integral, and to write

$$\bar{c}_{fw} = \int_0^L \frac{nqc(x)}{Q_{\text{tot}}}\, dx \tag{6}$$

where dx is an increment in lung height, L is the total height of the lung measured in cm from the apex (Table 1), $n(x)$ is the number of alveolar ducts emptying per unit height of lung tissue (assumed to be proportional to the transverse cross sectional area of the lung at position x), $q(x)$ is the mean gas volume flow rate, and $c(x)$ is the concentration present in the ADs located at position x. The flow-weighted average in Eq. 6 can be compared to the spatial average gas concentration, given by

$$\bar{c}_{sp} = \frac{1}{N} \int_0^L nc(x)\, dx \ . \tag{7}$$

TABLE 1. Regional properties of lung tissue used for the calculation of the volume flow-weighted average and the spatial average CO_2 concentrations according to Eqs. 6 and 7. x is the dimensionless position measured down from the lung apex and L is the dimensionless lung height.

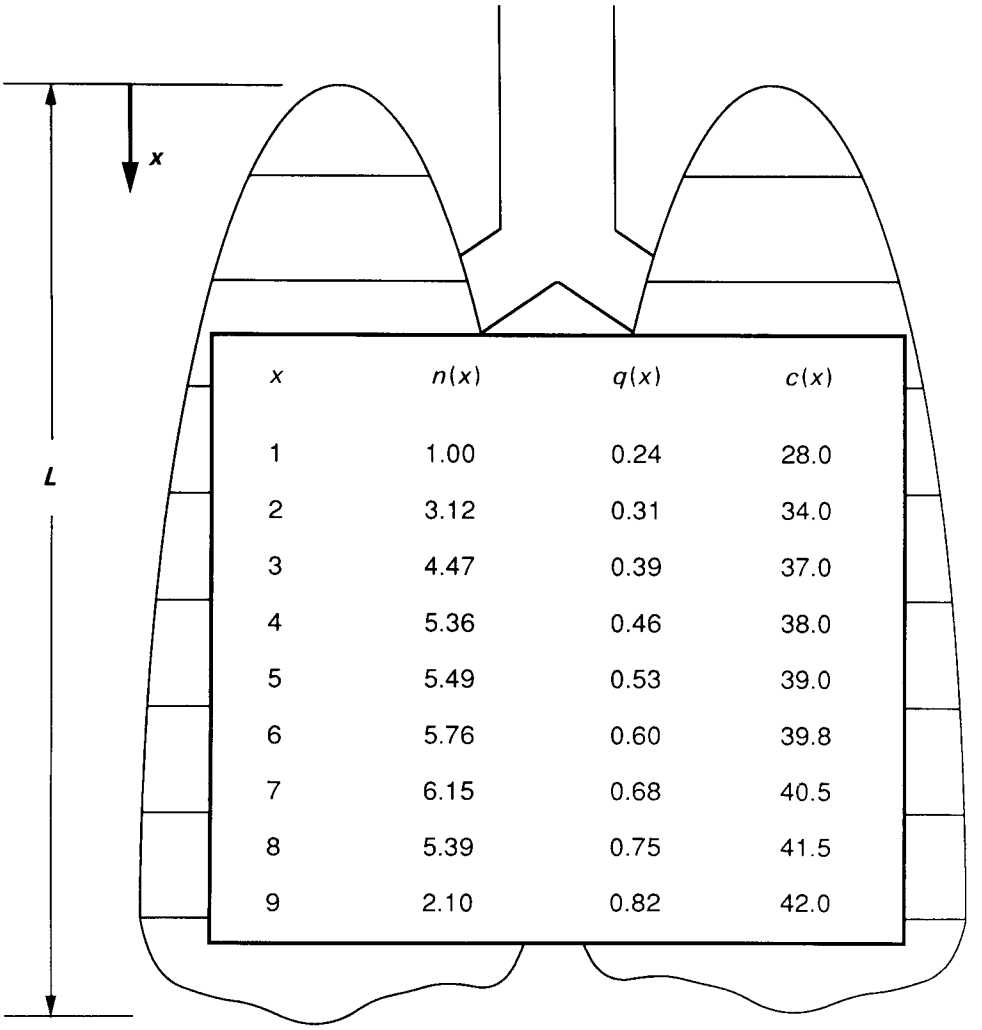

x	$n(x)$	$q(x)$	$c(x)$
1	1.00	0.24	28.0
2	3.12	0.31	34.0
3	4.47	0.39	37.0
4	5.36	0.46	38.0
5	5.49	0.53	39.0
6	5.76	0.60	39.8
7	6.15	0.68	40.5
8	5.39	0.75	41.5
9	2.10	0.82	42.0

When typical values for n, based on anatomical photographs (17), q, and c, based on regional gas exchange data (26), are substituted into Eq. 6 and Eq. 7 and the integrals are evaluated, one finds that the flow-weighted and spatial average concentrations differ by less than 2%. Since a spatial average CO_2 concentration is computed in the SPM, one would conclude that the SPM provides an adequate estimate of the actual volume flow-averaged CO_2 concentration at the mouth and within the airways at a given cumulative volume.

The second assumption of the SPM is supported by examining the degree of an-

atomic asymmetry that exists in the real respiratory airway system. Although there is considerable variation in path length between the carina and the respiratory bronchioles as reported by Horsfield and Cumming (11), who found a mean of 13 cm with a standard deviation ≅ 5 cm, the variation in path length along the acinus is much smaller. A recent study by Haefeli-Bleuer and Weibel found a mean acinar path length of 8.25 mm with a standard deviation of 1.41 mm (9). The difference in these variances is significant since 90% of airway volume is contained in the acini and the acinar path length deviation of 1.41 mm represents less than 2 generations out of a total of about 25 between the mouth and the end of the acini. Furthermore, the volume of these 2 generations of acinar airways is less than 10% of total acinar gas volume (including the volume of gas in the alveoli). When considered in terms of cumulative volume in from the mouth, the natural spatial parameter of gas washout, the deviation of the asymmetric airways from a single path is seen to be rather small.

CONCLUSION

The SPM is a simple but complete distributed parameter model of the complex phenomenon of gas-phase CO_2 transport from the lung periphery. The SPM has a small number of parameters that describe the main features of acinar anatomy and accurately simulates experimental results. The quantitative effects of independently varying breathing pattern, physiologic variables, and structural parameters on the shape of the steady state CO_2 washout curve reveal distinct relationships between model lung structure and function. Table 2 is a summary of the relationships between the SPM parameters and their effects on Phase III. The influence of V_T, $A(z)$, and D_{mol} on the slope of Phase III is clear. These findings may lead to a better understanding of small airways diseases.

TABLE 2. Phase III changes due to acinar parameter variations. Major and minor causes of changes of Phase III slope and $\dot{V}_{CO_2}$ in the SPM are listed. Major causes are in bold print and minor causes are in normal print.

To Increase Phase III Slope	To Decrease Phase III Slope
reduce V_T	**divert bloodflow proximally**
reduce $A(z)$ with lengthening	raise V_T
reduce gas diffusivity	reduce cardiac output
raise breathing frequency	reduce venous CO_2 tension
raise cardiac output	raise $A(z)$ with shortening
raise venous CO_2 tension	raise $A(z)$ without shortening
divert bloodflow distally	
reduce alveolar volume	
reduce $A(z)$ without lengthening	
To Increase Phase III Height	**To Decrease Phase III Height**
raise cardiac output	**reduce cardiac output**
raise venous CO_2 tension	**reduce venous CO_2 tension**
divert bloodflow proximally	reduce $A(z)$ with lengthening

REFERENCES

1. Bates, D.V.; Macklem, P.T.; Christie, R.V. Pulmonary emphysema. Philadelphia: W.B. Saunders Co.; 1971.
2. Buohuys, A. Respiratory dead space. In: Fenn, W.O.; Rahn, H., eds. Handbook of Physiology. Section 3: Respiration, Vol. I. Washington, D.C.: Am. Physiol. Soc.; 1964: pp. 699–714.
3. Cerretelli, P.; DiPrampero, P.E. Gas exchange in exercise. In: Fishman, A.P., ed. Handbook of Physiology, Section 3: The Respiratory System, Vol. IV. Washington, D.C.: Am. Physiol. Soc.; 1987: pp. 297–307.
4. Cherniak, R.M.; Cherniak, L. Respiration in health and disease. Philadelphia: W.B. Saunders Co.; 1983.
5. Chilton, A.B.; Stacey, R.W. A mathematical analysis of carbon dioxide respiration in man. Bull. Math. Biophysics. 14; 1952.
6. Cumming, G.; Horsfield, K.; Jones, J.G.; Muir, D.C.F. The influence of gaseous diffusion on the alveolar plateau at different lung volumes. Respir. Physiol. 2:386–398; 1967.
7. DuBois, A.B.; Britt, A.G.; Fenn, W.O. Alveolar CO_2 during the respiratory cycle. J. Appl. Physiol. 44:325; 1981.
8. Fletcher, R. The single breath test for carbon dioxide. Arlöv, Sweden: Gerlings; 1986. Thesis.
9. Haefeli-Bleuer, B.; Weibel, E.R. Morphometry of the human pulmonary acinus. Anatom. Rec. 220:401–414; 1988.
10. Hansen, J.E.; Ampaya, E.P.; Bryant, G.H.; Navin, J.J. Human air space shapes, sizes, areas, and volumes. J. Appl. Physiol. 38:990–995; 1975.
11. Horsfield, K.; Cumming, G. Morphology of the bronchial tree in man. J. Appl. Physiol. 24:373–383; 1968.
12. Luijendijk, S.C.M.; Zwart, A.; de Vries, W.R.; Salet, W.M. The sloping alveolar plateau at synchronous ventilation. Pflügers Arch. 384:267–277; 1980.
13. Marthar, R; Castaing, Y; Manier, G.; Guenard, H. Gas exchange alternations in patients with chronic obstructive lung disease. Chest 87(4): 470–475; 1985.
14. Neufeld, G.R.; Gobran, S.; Baumgardner, J.E.; Aukburg, S.J.; Schreiner, M.; Scherer, P.W. Diffusivity, respiratory rate, and tidal volume influence inert gas expirograms. Respir. Physiol. 84:31–47; 1991.
15. Paiva, M. Gas transport in the human lung. J. Appl. Physiol. 35:401–410; 1973.
16. Paiva, M.; Engel, L.A. The anatomical basis for the sloping N_2 plateau. Resp. Physiol. 44:325–337; 1981.
17. Rohen, J.W.; Yokochi, C. Colar atlas of anatomy. New York: Igaku-Shoin; 1988.
18. Scherer, P.W.; Gobran, S.; Aukburg, S.J.; Baumgardner, J.E.; Bartkowski, R.; Neufeld, G.R. Numerical and experimental study of steady-state CO_2 and inert gas washout. J. Appl. Physiol. 64:1022–1029; 1988.
19. Scherer, P.W.; Neufeld, G.R.; Aukburg, S.J.; Hess, G.D. Measurement of effective peripheral bronchial cross section from single-breath gas washout. J. Biomech. Eng. 104:290–293; 1983.
20. Scherer, P.W.; Haselton, F.R. Convective mixing in tube networks. AIChE J. 25:542–544; 1979.
21. Scherer, P.W.; Haselton, F.R. A network theory of bronchial gas mixing applied to single breath nitrogen washout. Lung. 158:201–220; 1980.
22. Scherer, P.W.; Shendalman, L.H.; Greene, N.M. Simultaneous diffusion and convection in single breath lung washout. Bull. of Math. Biophys. 34:393–412; 1972.
23. Smidt, U.; Worth, H. Diagnostik des Lungenemphysems auf expiratorischen CO_2-Partialdruckkurven mit Hilfe eines Mikroprozessors. Biomed. Technik. 22:357; 1977.
24. Ultman, J.S.; Blatman, H.S. Longitudinal mixing in pulmonary airways: Analysis of inert gas dispersion in symmetric tube network models. Resp. Physiol. 30:349–367; 1977.
25. Weibel, E.R. Morphometry of the human lung. Berlin: Springer-Verlag; 1963.
26. West, J.B. Respiratory physiology—The essentials. Baltimore: Wiliams and Wilkins; 1985.
27. West, J.B. Pulmonary pathophysiology—The essentials. Baltimore: Williams and Wilkins; 1987.
28. West, J.B.; Fowler, K.T.; Hugh-Jones, P.; O'Donell, T.V. The measurement of the inequality of ventilation and perfusion in the lung by analysis of single espirates. Clin. Sci. 16:549; 1957.
29. Worth, H.; Piiper, J. Diffusion of helium, carbon dioxide, and sulfur hexafluoride in gas mixtures similar to alveolar gas. Respir. Physiol. 32: 155–166; 1978.

NOMENCLATURE

$A(z)$ = total airway cross sectional area of generation z [cm^2]
$A_D(z)$ = total airway cross sectional area of generation z in diseased lung [cm^2]
AD = alveolar ducts
$A_H(z)$ = total airway cross sectional area of generation z in healthy lung [cm^2]
$c(x)$ = CO_2 concentration in lung tissue at position x measured from the lung apex [mm Hg]
$c(z,t)$ = CO_2 concentration in generation z at time t [cm^3 CO_2/cm^3, dimensionless]
c_B = CO_2 concentration in equilibrium with the pulmonary arterial blood [mm Hg]
$\bar{c}_{fw}$ = flow-weighted concentration average [mm Hg]
$\bar{c}_{sp}$ = spatial average concentration [mm Hg]
COPD = chronic obstructive pulmonary disease
D_{mol} = molecular diffusivity [cm^2/s]
d_D = airway diameter in generation z of diseased lung [cm]
d_H = airway diameter in generation z of healthy lung [cm]
f = breathing frequency [breaths per minute, bpm]
FRC = functional residual capacity [cm^3]
$l(z)$ = airway length in generation z [cm]
$n(x)$ = number of alveolar ducts per unit height of lung tissue [dimensionless]
N_A = number of alveoli in generation z [dimensionless]
$N_D(z)$ = number of alveoli in generation z in diseased lung [dimensionless]
$N_H(z)$ = number of alveoli in generation z in healthy lung [dimensionless]
N_T = total number of alveoli in Weibel lung [dimensionless]
$P_{A_{CO_2}}$ = alveolar CO_2 concentration [mm Hg]
$q(x)$ = mean gas volume flow rate per unit height of lung tissue [dimensionless]
$\dot{Q}(z,t)$ = volume flowrate through airways in generation z at time t [cm^3/s]
$\dot{Q}_B$ = total cardiac output [cm^3/s]
R = airway reduction factor [dimensionless]
SPM = single path model
$S(z,t)$ = alveolar capillary CO_2 emitted from blood in generation z at time t [cm^3/sec]
t = time [seconds]
$V(z)$ = airway volume of generation z [cm^2]
$V_A(z,t)$ = alveolar volume of generation z at time t [cm^3]
$V_{A,T}$ = total alveolar volume in lung at beginning of inspiration [cm^3]
V_c = volume of conducting airways in generations 0–4 [cm^3]
$\dot{V}_{CO_2}$ = CO_2 excretion [cm^3/min]
V_T = tidal volume inhaled at mouth [ml]
x = position in lung measured from apex [dimensionless]
z = generational coordinate [dimensionless]
Δz = finite increment in generational coordinate [dimensionless]
α = alpha = FRC_D/FRC_H, ratio of diseased to healthy functional residual capacity [dimensionless]
β = beta = ratio of diseased to healthy airspace diameters, d_D/d_H
λ = lambda = CO_2 solubility in blood [cm^3 CO_2 dissolved/cm^3 blood/CO_2 concentration over blood, dimensionless]